coatings

MDPI

Communication

Preparation of High Entropy Alloys Without Pre-Alloying, Using Laser Melt Deposition (LMD) Technique

Ferenc Hareancz [1,2,3], Gergely Juhász [1,2,3], Márk Windisch [1,4], Anita Heczel [1] and Ádám Vida [1,*]

[1] Bay Zoltán Nonprofit Ltd. for Applied Research, Kondorfa Street 1, 1116 Budapest, Hungary; ferenc.hareancz@bayzoltan.hu (F.H.); gergely.juhasz@bayzoltan.hu (G.J.); mark.windisch@bayzoltan.hu (M.W.); anita.heczel@bayzoltan.hu (A.H.)
[2] Department of Innovative Vehicles and Materials, GAMF Faculty of Engineering and Computer Science, John Von Neumann University, Izsáki Street 10, 6000 Kecskemét, Hungary
[3] Doctoral School on Materials Sciences and Technologies, Óbuda University, Népszínház Street 8, 1081 Budapest, Hungary
[4] Department of Materials Physics, Eötvös Loránd University, Pázmány Péter Promenade 1/A, 1117 Budapest, Hungary
* Correspondence: adam.vida@bayzoltan.hu; Tel.: +36-70-515-7182

Abstract: This study explores the fabrication of an equimolar CoCrFeNi high-entropy alloy (HEA) using laser metal deposition (LMD) technique on a 316 L austenitic stainless steel substrate, without pre-alloying. Elemental metal powders were mixed in a planetary ball mill and directly deposited to investigate the effect of layer number on alloy composition and substrate intermixing. Experimental results revealed significant dilution in the first four layers, with substrate intermixing affecting composition. The coarse-grained crystal structure observed in the initial layers persisted in subsequent layers, and hardness measurements indicated the cumulative thermal effects of sequential deposition. From an industrial perspective, this approach offers a cost-effective and flexible manufacturing strategy, eliminating the need for pre-alloying. Moreover, gradient compositional layers can be achieved, enabling tailored material properties. This work demonstrates the feasibility of producing multi-layer HEAs directly from elemental powders while addressing the challenges of compositional stability.

Keywords: high entropy alloy; laser metal deposition; gradient compositional layers; CoCrFeNi

check for updates

Academic Editor: Fanli Kong

Received: 23 December 2024
Revised: 17 January 2025
Accepted: 19 January 2025
Published: 21 January 2025

Citation: Hareancz, F.; Juhász, G.; Windisch, M.; Heczel, A.; Vida, Á. Preparation of High Entropy Alloys Without Pre-Alloying, Using Laser Melt Deposition (LMD) Technique. *Coatings* **2025**, *15*, 116. https://doi.org/10.3390/coatings15020116

Copyright: © 2025 by the authors. Licensee MDPI, Basel, Switzerland. This article is an open access article distributed under the terms and conditions of the Creative Commons Attribution (CC BY) license (https://creativecommons.org/licenses/by/4.0/).

1. Introduction

High-entropy alloys (HEAs) represent a novel alloying system distinct from traditional alloys, containing 4–5 principal elements at concentrations of 5–35 atomic percent. Unlike conventional alloys, HEAs exhibit a remarkable property of forming solid solutions, preventing the formation of complex compounds or intermetallic phases, thereby enhancing their toughness. Among these alloys, CoCrFeNi-based HEAs have garnered significant attention due to their face-centered cubic (FCC) crystal structure, which balances ductility and corrosion resistance [1–3].

The primary objective of our scientific experiments is to advance the industrial applicability and development of HEAs. While prior studies have produced deposited HEA layers from pre-alloys, this approach is time-consuming and costly [1,4,5]. The laser metal deposition (LMD) technology employed in this research enables the direct implementation of elemental metal powders into the surface melt pool [6–8]. This technique offers a significant competitive advantage and cost efficiency, making HEAs more viable for various industries [5].

Recent advancements in LMD-produced CoCrFeNi alloys highlight their potential in applications demanding high strength, ductility, and corrosion resistance. Incorporating secondary phases or tailored chemical modifications, such as adding Mo or Al, has shown promise for optimizing mechanical properties and environmental durability. However, understanding the impact of microstructural changes on anisotropy and grain morphology under varying deposition parameters and thermal gradients remains a challenge [9–13]. Although several studies of HEAs deposited by LMD on steels have been reported in the literature, there is a lack of or no trend to investigate the fundamental properties of multilayered coatings deposited using a layer-by-layer method [14–16]. Situations where multiple layers need to be deposited are abundant in industrial applications [17–19]. Therefore, in this study, we investigate, in a first approximation, whether a solid solution with a continuous grain morphology is formed when 10 layers are deposited. Significant mixing with the substrate is expected in the first few layers; therefore, several layers are required to form a homogeneous, high-entropy alloy deposit. Examining the composition of the deposit layers helps to understand how to minimize the number of deposit cycles without compromising the final layer composition. The ten layers ensure that sufficient thickness can be tested to determine the transition from mixing to the desired composition. We investigate whether chemical separation or possible dilution occurs and examine how the layer hardness evolves as a function of the layers.

2. Materials and Methods

2.1. Sample Processing

In our experiments, a CoCrFeNi equiatomic metal powder mixture was produced with precise weighting, followed by homogenization in a planetary mill. Layers were then deposited onto a 12 mm thick 316 L austenitic stainless steel substrate using laser metal deposition technology.

Metal powders with different grain sizes were used. The grain sizes of the powders were determined by Scanning Electron Microscopy (SEM) measurements using the image analysis software ImageJ version 1.54g (National Institutes of Health, Bethesda, MD, USA). The average grain sizes are shown in Table 1.

Table 1. Average particle sizes and median sizes of metal powers used.

Element	Average Size (µm)	Median Size (µm)
Co	71	68
Cr	44	44
Fe	40	39
Ni	5	5

Due to the differences in grain sizes, the metal powders were mixed in a Fritsch Vario-Planetary Mill (Fritsch, Idar-Oberstein, Germany) for 90 min. The main plate rotated at 700 rpm, and the planetary bowl at 120 rpm. The resulting powder mixture was loaded into a GTV PF 2/2 LC powder feeder (GTV, Luckenbach, Germany) connected to a disc laser, as described below. For powder dispersion, 4.6 argon was used as a carrier gas.

The experiments were conducted using a Trumpf TruLaser Cell 7020, a CNC-controlled laser processing device (Trumpf SE + Co. KG, Ditzingen, Germany). The processing head included an MSO 70 three-jet nozzle, using 4.6 argon as a shielding gas. The laser source was a TruDisc 4001 equipped with a dual-core fiber optic cable (Trumpf SE + Co. KG, Ditzingen, Germany).

The following parameters were applied during laser deposition:

- Laser power: 1750 W;

- Scanning speed: 850 mm/min;
- Focus spot size: 3 mm;
- Powder feeder disc speed: 4 rpm;
- Overlap: 60%;
- Ar flow: 7 L/min.

The layer deposition was performed with consistent disc rotation speed and carrier gas flow rate. The deposition strategy is illustrated in Figure 1.

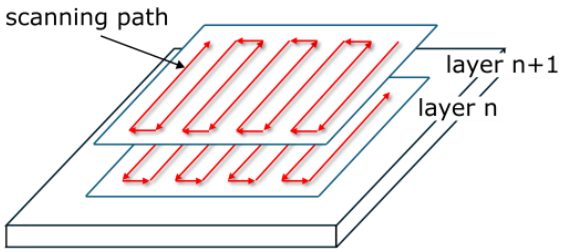


Figure 1. The scanning strategy.

During the experiments, single and multiple layers (10 layers stacked on each other) were deposited; the deposition strategy was different for even and odd layers, as shown in Figure 1.

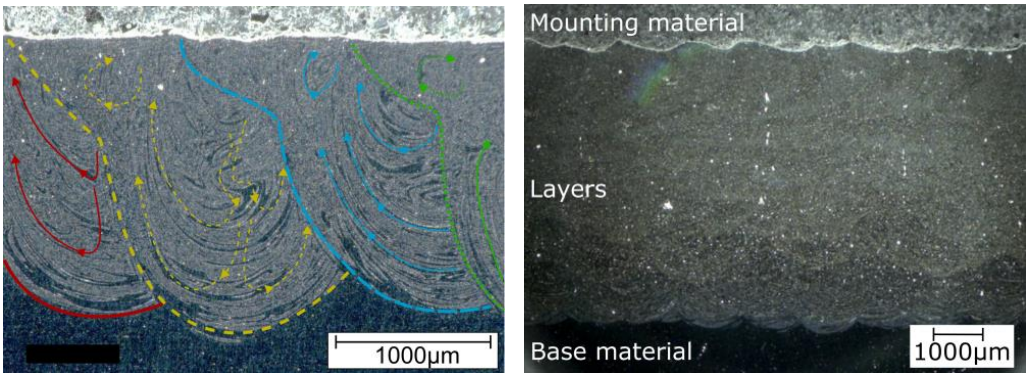
2.2. Sample Preparation and Analysis

The deposited area measured 30 mm × 30 mm with varying heights. To prepare the samples for analysis, they were sectioned perpendicularly to the deposition path and further subdivided into smaller pieces. For cross-sectional examination, the samples underwent a precise polishing process. After grinding with a standard grit paper series, a diamond suspension with particle sizes of 3 µm and 1 µm was employed, followed by a final polishing step using a 0.05 µm Al_2O_3 suspension.

The microstructural characteristics, chemical composition, and crystallographic properties of the samples were analyzed using a SEM equipped with energy-dispersive spectrometry (EDS) and electron backscatter diffraction (EBSD) detectors. EBSD measurements were performed at an accelerating voltage of 20 keV, while EDS measurements utilized a 15 keV accelerating voltage. The hardness was assessed using the Vickers method, applying a load of 1 kgf.

3. Results and Discussion

The deposited layers were first examined with an optical microscope. Figure 2a shows how the CoCrFeNi alloy is mixed with the substrate, with the directions of the Marangoni current marked in the figure [20,21]. Marangoni flow, driven by surface tension gradients in the molten pool during LMD, enhances mixing between the deposited powder and substrate material. It creates strong convection currents that evenly distribute alloying elements, ensuring a uniform composition and reducing defects like porosity. Figure 2b shows that the deposited layers can be considered dense, as they do not contain significant porosity or voids that could negatively affect the mechanical properties of the layer. This flow also improves bonding between layers in multi-layer builds and influences the solidification dynamics, leading to better grain structures and mechanical properties. Optimizing process parameters can effectively harness Marangoni flow to enhance the quality of LMD components [22].

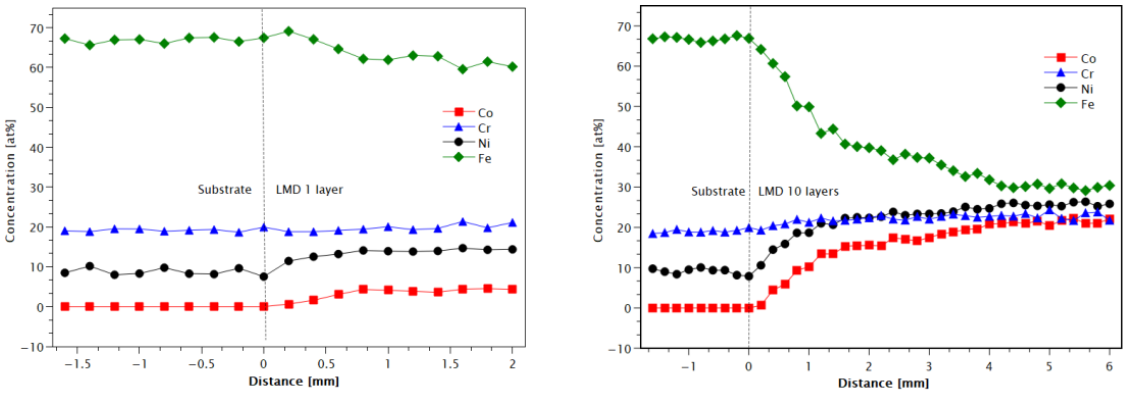


(**a**) (**b**)

Figure 2. Optical microscope image of ground and polished samples (**a**) 1 layer; (**b**) 10 layers.

The thickness of the deposited layer relative to the substrate was measured using an optical microscope and SEM, and the depth of the melted substrate layer was calculated based on EDS data. The substrate material exhibited a melting depth of 1.2–1.6 mm, while the thickness of the deposited layers was consistently 0.45 mm. However, EDS measurements alone are insufficient to precisely determine the dimensions of the deposited layer and the extent of the dilution zone.

SEM-EDS measurements reveal that the intended HEA composition, as defined in the powder state, is not achieved in the first layer due to the extensive melting of the base material required for strong adhesion. The substrate and the deposited layer have different compositions, so they are highly intermixed during laser melting. Each new layer builds on the previous mix and further blends to approximate the intended composition until the intended layer composition is achieved. While reducing the remelted layer thickness could minimize this dilution effect, it may compromise the adhesion quality of the deposited layer. As the aim of our study was to show whether the HEA solid solution with a coherent crystal structure is formed by 10 layers, we melt the base plate deeply, which is also reflected in laser performance data. The dilution effect is confirmed by the measurement results shown in Figure 3a.



(**a**) (**b**)

Figure 3. EDS measurement results (**a**) for 1 layer; (**b**) for 10 layers.

For the 10-layer sample, the EDS measurement shows a 2.5 mm wide transition layer where the alloying elements are continuously enriched, as shown in Figure 3b. Significant substrate mixing was observed in the first four layers due to deep melting of the base material to ensure strong adhesion. This mixing led to a dilution effect, with iron (Fe) from the substrate remaining dominant in the composition. However, as successive layers were

deposited, the influence of substrate mixing diminished, and the elements of the CoCrFeNi alloy became more prevalent. The successful fabrication of a 10-layer CoCrFeNi HEA directly from a mixture of elemental powders without pre-alloying indicates the potential of the LMD manufacturing technique. On the other hand, this approach is also excellent for building an HEA layer even without a cushion layer on a substrate whose crystal structure is not necessarily compatible with the crystal structure of the layer that is formed [23,24].

Figure 4a,b show inverse pole figure (IPF) maps obtained via EBSD for the 1-layer and 10-layer samples, respectively. Only the FCC phase was detected in the EBSD measurement. The grains are bounded by high-angle grain boundaries (HAGBs) with misorientations greater than 10°. The EBSD images clearly indicate that the grain morphology is predominantly columnar. These grains grew epitaxially from the melt pool boundaries upwards along the LMD building direction, forming a solid solution. In the upper layers, the direction of grain bending reflects the sequential scanning bands, which align with the thermal gradient direction [25,26]. It is possible to distinguish the steel substrate and the HEA layer to study the interface based on the EBSD measurements (see Figure 4c). Both the 316 L steel substrate and the CoCrFeNi HEA share the same FCC crystal structure, with very similar lattice constants, and no residual stresses were detected at the interface [27,28].

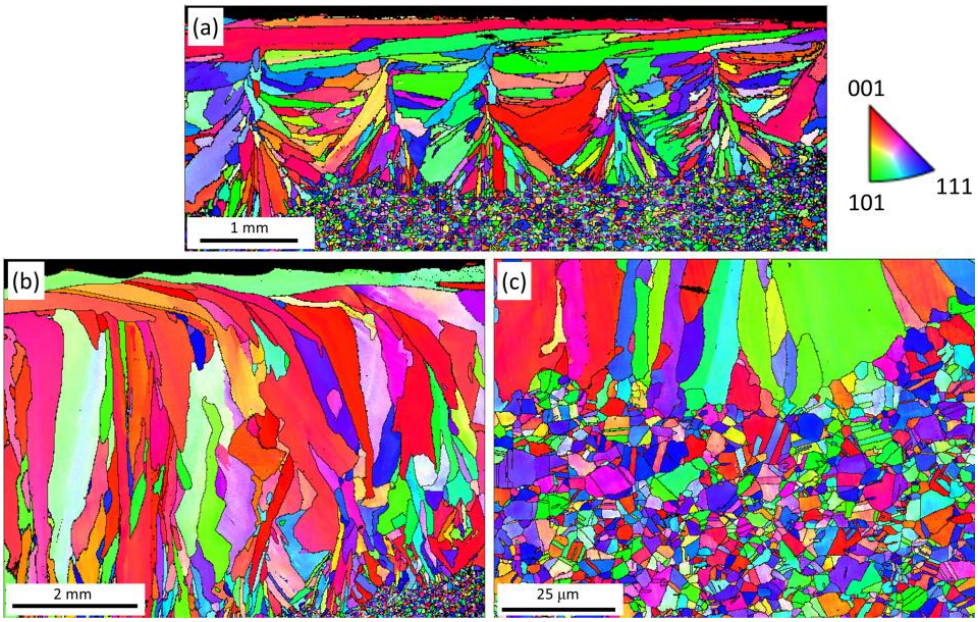


Figure 4. EBSD-based orientation images (**a**) of 1 layer; (**b**) of 10 layers; (**c**) of melted zone border between substrate and first layer.

The EBSD measurements provide a detailed characterization of the microstructure, which directly influences the material's hardness. For the single deposited layer, there is minimal variation in hardness between the substrate and the LMD layer. In the single deposited layer, the substrate hardness changes due to the applied heat, with the substrate hardness of 170 HV decreasing slightly and then increasing to 190 HV near the deposited layer, as shown in Figure 5a. As a result of the dilution, the layer hardness suddenly decreases to 170 HV.

Figure 5b shows the 10-layer deposit. Due to the cumulative thermal effects of the deposition process, the substrate undergoes full heat treatment, and its hardness decreases to 158 HV. Similar to the single deposited layer, the hardness drops sharply in the initial layers. At the same time, the deposited layers gradually harden through interactions with the underlying layers. Near the topmost layers, the highest hardness values are observed, presumably due to faster cooling occurring in these regions.

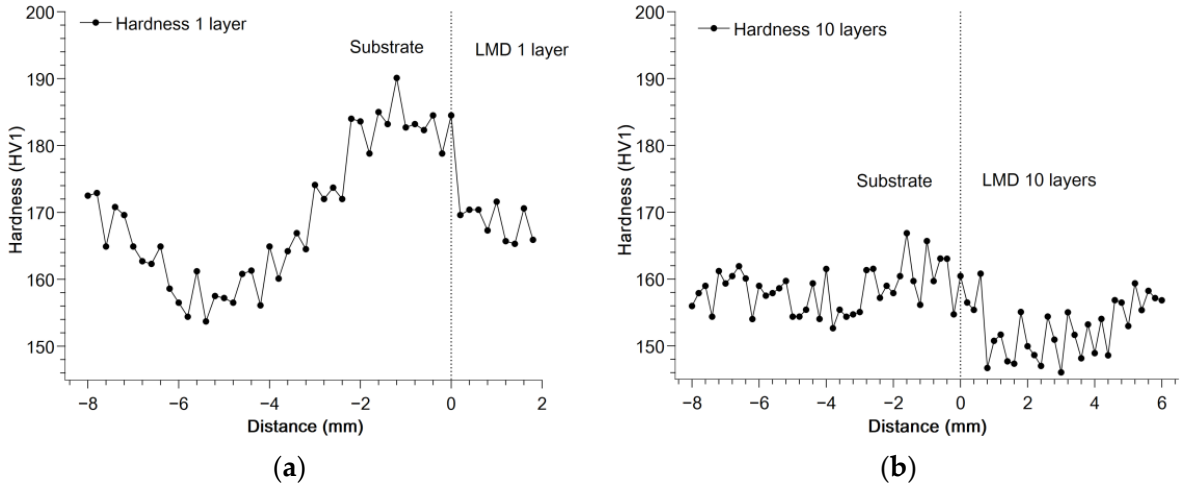


Figure 5. Hardness measurements (**a**) for 1 layer; (**b**) for 10 layers.

4. Conclusions

1. The processing of coatings using the LMD technique, which involves employing a mixture of elemental powders during deposition, must take into account that the initial layers will not precisely reflect the elemental composition calculated from the powder mass measurements. By layers 5 and 6, the desired elemental distribution and composition are achieved, closely approximating the composition of a CoCrFeNi powder mixture. From this point forward, the alloy can be considered a high-entropy alloy (HEA).
2. The Electron Backscatter Diffraction (EBSD) analysis revealed a predominantly columnar grain structure aligned with the build direction, suggesting that the thermal gradients inherent in the LMD process influenced grain growth. This observation aligns with findings in similar studies, where directional solidification during LMD leads to columnar grain structures [29]. Based on the combined results from EBSD and EDS analyses, it can be concluded that using LMD to deposit HEA coatings produces a homogeneous solid solution in the deposited layers.
3. Hardness measurements revealed similar values for the substrate and the CoCrFeNi alloy. However, repeated thermal cycling in multi-layer deposition led to slight softening, aligning with known effects of heat accumulation and resulting microstructural changes [29].
4. This study demonstrates the viability of producing multi-layer HEAs directly from elemental powders using LMD, achieving a solid solution with coherent crystal structures. The findings contribute to the understanding of compositional stability and microstructural evolution in additively manufactured HEAs, paving the way for their broader application in various industries. This approach not only simplifies the production process but also allows for the creation of gradient compositional layers, enabling tailored material properties for specific industrial applications.

Author Contributions: F.H.: conceptualization, methodology, writing—original draft preparation, writing—review and editing, visualization. G.J.: conceptualization, methodology, validation, formal analysis. M.W.: investigation, software, validation, visualization, writing—review and editing. A.H.: investigation, software, validation, visualization, writing—review and editing, supervision. Á.V.: conceptualization, methodology, writing—review and editing, visualization, supervision, project administration, funding acquisition. All authors have read and agreed to the published version of the manuscript.

Funding: This work is funded by the KDP-2021 Program of the Ministry of Innovation and Technology from the source of the National Research, Development and Innovation Fund.

Institutional Review Board Statement: Not applicable.

Informed Consent Statement: Not applicable.

Data Availability Statement: Data are contained within the article.

Acknowledgments: The authors express their gratitude to Richárd Bak for his invaluable contribution to the preparation of the elemental powder mixtures, ensuring the quality and consistency necessary for this study. Special thanks are also extended to Anna Maloveczky for her exceptional assistance in metallographic sample preparation, which was critical for the successful execution of the microstructural analyses. Their expertise and support significantly enhanced the quality of this research.

Conflicts of Interest: Authors Ferenc Hareancz, Gergely Juhász, Márk Windisch, Anita Heczel, and Ádám Vida were employed by the company Bay Zoltán Nonprofit Ltd. for Applied Research. The authors declare that the research was conducted in the absence of any commercial or financial relationships that could be construed as a potential conflict of interest.

References

1. Chao, Q.; Guo, T.; Jarvis, T.; Wu, X.; Hodgson, P.; Fabijanic, D. Direct laser deposition cladding of Al CoCrFeNi high entropy alloys on a high-temperature stainless steel. *Surf. Coat. Technol.* **2017**, *332*, 440–451. [CrossRef]
2. Cantor, B.; Chang, I.T.H.; Knight, P.; Vincent, A.J.B. Microstructural development in equiatomic multicomponent alloys. *Mater. Sci. Eng. A* **2004**, *375–377*, 213–218. [CrossRef]
3. Yeh, J.-W.; Chen, S.-K.; Lin, S.-J.; Gan, J.-Y.; Chin, T.-S.; Shun, T.-T.; Tsau, C.-H.; Chang, S.-Y. Nanostructured High-Entropy Alloys with Multiple Principal Elements: Novel Alloy Design Concepts and Outcomes. *Adv. Eng. Mater.* **2004**, *6*, 299–303. [CrossRef]
4. Tang, Y.; Wan, N.; Shen, M.; Jiao, H.; Liu, D.; Tang, X.; Zhao, L. A comparison of the microstructures and hardness values of non-equiatomic (FeNiCo)-(AlCrSiTi) high entropy alloys having thermal histories related to laser direct metal deposition or vacuum remelting. *J. Mater. Res. Technol.* **2021**, *15*, 696–707. [CrossRef]
5. Tang, Y.; Wang, W.; Wan, N.; Tang, X.; Jiao, H.; Liu, D.; Hu, Y.; Zhao, L. Solidification and tribological behaviors of CoCrFeNiSi0.5-(Al,Ti) non-equiatomic high entropy alloy coatings fabricated by direct laser deposition. *Surf. Coat. Technol.* **2024**, *483*, 130808. [CrossRef]
6. Taghizadeh, M.; Zhu, Z.H. A comprehensive review on metal laser additive manufacturing in space: Modeling and perspectives. *Acta Astronaut.* **2024**, *222*, 403–421. [CrossRef]
7. Pandey, V.; Seetharam, R.; Chelladurai, H. A comprehensive review: Discussed the effect of high-entropy alloys as reinforcement on metal matrix composite properties, fabrication techniques, and applications. *J. Alloys Compd.* **2024**, *1002*, 175095. [CrossRef]
8. Leyens, C.; Beyer, E. Innovations in laser cladding and direct laser metal deposition. In *Elsevier eBooks*; Elsevier: Amsterdam, The Netherlands, 2014; pp. 181–192. [CrossRef]
9. Xiang, S.; Luan, H.; Wu, J.; Yao, K.-F.; Li, J.; Liu, X.; Tian, Y.; Mao, W.; Bai, H.; Le, G.; et al. Microstructures and mechanical properties of CrMnFeCoNi high entropy alloys fabricated using laser metal deposition technique. *J. Alloys Compd.* **2018**, *773*, 387–392. [CrossRef]
10. Radhakrishnan, M.; Sharma, S.; Palaniappan, S.; Pantawane, M.V.; Banerjee, R.; Joshi, S.S.; Dahotre, N.B. Influence of Thermal Conductivity on Evolution of Grain Morphology during Laser-based Directed Energy Deposition in CoCrxFeNi High Entropy Alloys. *Addit. Manuf.* **2024**, *92*, 104387. [CrossRef]
11. Tan, J.; Peng, K.; Chen, X.; Tong, Z.; Chen, C.; Zhang, H. Laser metal deposition of CoCrFeNi(SiC)x high-entropy alloys: Microstructure and mechanical properties. *J. Mater. Res. Technol.* **2024**, *32*, 3831–3841. [CrossRef]
12. Zhang, B.; Mu, W.; Cai, Y. A novel strategy to regulate the precipitation-strengthened high-entropy alloy fabricated by laser directed energy deposition. *Mater. Charact.* **2024**, *215*, 114191. [CrossRef]
13. Jiang, G.; Chen, Z.; Liu, C.; Li, H.; Guo, C.; Yang, Z.; Sun, W.; Tong, Y.; Chen, W.; Tang, H.; et al. Recrystallization and twinning enhancing mechanical property of laser directed energy deposited CoCrFeNi high entropy alloys induced by synchronous ultrasonic impact. *Addit. Manuf.* **2024**, *93*, 104410. [CrossRef]
14. Zhang, Y.; Zhao, Y.; Sun, L.; Wang, L.; Li, L.; Zhan, X. Formation mechanism of AlNbTiVZr high entropy alloy/Ti multi-principal element alloy by laser direct energy deposition: Microstructure evaluation and mechanical properties. *J. Alloys Compd.* **2024**, *997*, 174782. [CrossRef]

15. Chew, Y.; Bi, G.J.; Zhu, Z.G.; Ng, F.L.; Weng, F.; Liu, S.B.; Nai, S.M.L.; Lee, B.Y. Microstructure and enhanced strength of laser aided additive manufactured CoCrFeNiMn high entropy alloy. *Mater. Sci. Eng. A* **2018**, *744*, 137–144. [CrossRef]
16. Xue, P.; Zhu, L.; Xu, P.; Ren, Y.; Xin, B.; Wang, S.; Yang, Z.; Ning, J.; Meng, G.; Liu, Z. CrCoNi medium-entropy alloy thin-walled parts manufactured by laser metal deposition: Microstructure evolution and mechanical anisotropy. *Mater. Sci. Eng. A* **2021**, *817*, 141306. [CrossRef]
17. Dada, M.; Popoola, P.; Adeosun, S.; Mathe, N. High entropy alloys for aerospace applications. In *IntechOpen eBooks*; IntechOpen: London, UK, 2019. [CrossRef]
18. Yang, Y.-F.; Hu, F.; Xia, T.; Li, R.-H.; Bai, J.-Y.; Zhu, J.-Q.; Xu, J.-Y.; Zhang, G.-F. High entropy alloys: A review of preparation techniques, properties and industry applications. *J. Alloys Compd.* **2024**, *1010*, 177691. [CrossRef]
19. Adegbite, M.; Tiamiyu, A.A. Substitutional effects of Al and Mn on the microstructure and mechanical response of Cantor-derived high-entropy alloys for nuclear structural applications. *Mater. Sci. Eng. A* **2024**, *923*, 147674. [CrossRef]
20. Zhang, S.; Yao, C.; Zhang, D.; Liu, W.; He, L.; Du, D.; Sun, B.; Dong, A.; Zhang, B.; Xiong, L. Dynamics of pore formation and evolution during multi-layer directed energy deposition additive manufacturing via in-situ synchrotron X-ray imaging: A case study on high-entropy Cantor alloy. *Int. J. Mach. Tools Manuf.* **2024**, *200*, 104181. [CrossRef]
21. Le, T.-N.; Lo, Y.-L. Effects of sulfur concentration and Marangoni convection on melt-pool formation in transition mode of selective laser melting process. *Mater. Des.* **2019**, *179*, 107866. [CrossRef]
22. Wang, L.; Guan, X.; Yang, X.; Zhan, X.; Cai, X.; Shi, B. Thermal-fluid behavior and microstructure morphology during laser melting deposition of TiC/Ti6Al4V functionally graded materials. *J. Mater. Res. Technol.* **2023**, *27*, 3214–3230. [CrossRef]
23. Lu, K.; Zhu, J.; Ge, W.; Hui, X. Progress on new preparation methods, microstructures, and protective properties of High-Entropy Alloy coatings. *Coatings* **2022**, *12*, 1472. [CrossRef]
24. Feng, C.; Guan, Z.; Nan, S.; Xiao, M.; Liao, W.; Zhang, F. Effect of interface on nanostructure growth of high-entropy alloy and its excellent cushioning properties. *Mater. Today Commun.* **2024**, *39*, 109302. [CrossRef]
25. Liu, Z.; Zhu, Q.; Zhang, X. Tailoring microstructure and mechanical property of laser powder deposited Inconel 718 superalloy via hybrid processing strategies. *J. Manuf. Process.* **2021**, *68*, 1837–1848. [CrossRef]
26. Parimi, L.L.; Ravi, G.A.; Clark, D.; Attallah, M.M. Microstructural and texture development in direct laser fabricated IN718. *Mater. Charact.* **2014**, *89*, 102–111. [CrossRef]
27. Wang, Z.; Wu, Q.; Zhou, W.; He, F.; Yu, C.; Lin, D.; Wang, J.; Liu, C.T. Quantitative determination of the lattice constant in high entropy alloys. *Scr. Mater.* **2018**, *162*, 468–471. [CrossRef]
28. Zhou, X.; Curtin, W.A. First principles study of the effect of hydrogen in austenitic stainless steels and high entropy alloys. *Acta Mater.* **2020**, *200*, 932–942. [CrossRef]
29. Sun, M.; Liu, G.; Wei, W.; Zhou, L.; Li, J.; Tu, Q. Microstructures, Mechanical and High-Temperature tribological properties of Dual-Phase FE50MN30CO10CR10 High-Entropy alloy fabricated by laser metal deposition. *JOM* **2023**, *75*, 4138–4149. [CrossRef]

Disclaimer/Publisher's Note: The statements, opinions and data contained in all publications are solely those of the individual author(s) and contributor(s) and not of MDPI and/or the editor(s). MDPI and/or the editor(s) disclaim responsibility for any injury to people or property resulting from any ideas, methods, instructions or products referred to in the content.